# Investigating the oxidation mechanism of tantalum nanoparticles at high heating rates

Jeffery B. DeLisio, Xizheng Wang, Tao Wu, Garth C. Egan, Rohit J. Jacob, and Michael R. Zachariah

---

**Articles you may be interested in**

---

# Investigating the oxidation mechanism of tantalum nanoparticles at high heating rates

Jeffery B. DeLisio, Xizheng Wang, Tao Wu, Garth C. Egan, Rohit J. Jacob, and Michael R. Zachariah
*Department of Chemistry and Biochemistry and Department of Chemical and Biomolecular Engineering, University of Maryland, College Park, Maryland 20742, USA*

Reduced diffusion length scales and increased specific surface areas of nanosized metal fuels have recently demonstrated increased reaction rates for these systems, increasing their relevance in a wide variety of applications. The most commonly employed metal fuel, aluminum, tends to oxidize rapidly near its melting point (660 °C) in addition to undergoing a phase change of the nascent oxide shell. To further expand on the understanding of nanosized metal fuel oxidation, tantalum nanoparticles were studied due to their high melting point (3017 °C) in comparison to aluminum. Both traditional slow heating rate and *in-situ* high heating rate techniques were used to probe the oxidation of tantalum nanoparticles in oxygen containing environments in addition to nanothermite mixtures. When oxidized by gas phase oxygen, the oxide shell of the tantalum nanoparticles rapidly crystallized creating cracks that may attribute to enhanced oxygen diffusion into the particle. In the case of tantalum based nanothermites, oxide shell crystallization was shown to induce reactive sintering with the metal oxide resulting in a narrow range of ignition temperatures independent of the metal oxide used. The oxidation mechanism was modeled using the Deal-Grove model to extract rate parameters, and theoretical burn times for tantalum based nanocomposites were calculated. *Published by AIP Publishing.* https://doi.org/10.1063/1.4995574

## I. INTRODUCTION

Metal fuels possess higher energy densities than standard CHNO based energetics but traditionally suffer from slow reaction kinetics.[1–3] However, reduced diffusion length scales and increased specific surface areas of nanosized components have recently demonstrated increased reaction rates for these systems.[1,4] Most metal nanoparticles are passivated by a thin (typically 3–5 nm) nascent oxide shell, creating a barrier between the metal fuel and any oxidizer.[5] As the particle size decreases, the mass fraction of metal oxide makes up a significant percentage of the particle. Understanding the interaction between the metal core and the metal oxide shell is crucial in understanding the oxidation mechanism of the system.[6,7]

Aluminum is the most commonly used metal fuel due to its favorable energy density, low cost, and ignition characteristics.[2] Its oxidation mechanism has been extensively studied, and two prominent mechanisms for the ignition of Al nanoparticles (nAl) have been proposed: a diffusion based mechanism where the oxidizer and aluminum diffuse through the oxide shell boundary[8–10] and a melt dispersion based mechanism[11] where there is a violent rupturing of the oxide shell followed by spallation of the aluminum core. Previous studies have shown that decreasing the particle size of the fuel can dramatically decrease the ignition temperatures of Al based nanocomposites with the minimum recorded ignition temperatures being near the aluminum melting point.[10,12] High heating rate experiments have also shown that sintering of Al can occur on similar timescales as chemical reaction.[13,14]

A relatively recent development is the commercial availability of nanopowders of a wide variety of metals. In this study, tantalum (Ta) nanopowder was chosen due to its high melting point in comparison to Al, 3017 °C vs 660 °C. It is known that the crystallization of the aluminum oxide shell ($Al_2O_3$) is an important part of the Al ignition mechanism.[7,15,16] Unfortunately, this is a difficult process to thoroughly investigate because oxide crystallization occurs at a temperature very close to the melting point of Al.[7] Analogously, it has been observed that amorphous to crystalline transition in $Ta_2O_5$ thin films begins at ∼500 °C with crystallization occurring rapidly at higher temperatures;[17] however unlike Al, the effect of the oxide shell crystallization on ignition of tantalum nanopowders (nTa) can be probed without interference from melting.

Ta/tungsten oxide ($WO_3$) thermite composites prepared by sol-gel synthesis and spark plasma sintering have been previously studied, but these composites employed micron-sized (5 μm average particle size) tantalum.[18–20] In our work, the oxidation of nTa (<50 nm average particle size) in an aerobic environment at both low and high heating rates was studied in addition to the reaction mechanisms of several tantalum based nanothermites at high heating rates. These experiments were used to examine the oxidation of nTa strictly by a gas phase oxidizer ($O_{2(g)}$) in addition to a condensed phase oxidizer (metal oxide) in a nanothermite mixture. Thermogravimetric analysis and differential scanning calorimetry (TGA/DSC) were employed to investigate the oxidation of Ta and Al nanopowders at slow heating rates. Temperature jump (T-Jump) ignition and high heating rate transmission electron microscopy (TEM) experiments were performed to examine the ignition behavior of Ta nanopowders (nTa) in the presence of oxygen, in addition to Ta based nanothermites in vacuum. Ta ignition was observed well below the melting points of Ta

and tantalum oxide ($Ta_2O_5$), 3017 and 1872 °C, respectively. The experimental results allude to an oxygen diffusion dominated oxidation mechanism as the metal fuel is immobile prior to measured ignition temperatures. High heating rate TEM experiments also show two distinct oxidation mechanisms occurring depending on the maximum temperature achieved in the respective experiment.

## II. EXPERIMENTAL

### A. Materials

nAl (∼50 nm) was purchased from Novacentrix with an active Al content of 81% by mass, determined by thermogravimetric analysis (TGA) as stated by the manufacturer. The nTa (<50 nm) used in this study was purchased from Global Advanced Metals. All metal oxide nanopowders (<50 nm) used in Ta based thermite mixtures for T-Jump and TEM analysis were purchased from Sigma Aldrich. Stoichiometric thermite suspensions were prepared by physically mixing Ta with the corresponding metal oxide in hexane (T-Jump) or ethanol (TEM) and sonication for 30 min. Because nTa disperses poorly in hexane, and it is actually an aid in the coating of highly concentrated nTa particles on the T-Jump filament. nTa is much more easily dispersed in ethanol and was used as the carrier solvent of low concentrations of particles needed for TEM sample deposition.

### B. TGA/DSC characterization

Thermogravimetric analysis and differential scanning calorimetry (TGA/DSC) were performed using a TA Instruments SDT Q600. For both nTa and nAl oxidation analysis runs, a heating rate of 20 °C/min and an $O_2$ flow rate of 100 mL/min were employed.

### C. T-Jump ignition

A home built temperature jump (T-Jump) thin platinum (Pt) wire ignition source was used with a heating rate of ∼$10^5$ K/s.[21,22] The 76 $\mu$m diameter Pt wire was rapidly joule heated with a 3 ms current pulse, while a high-speed video was taken at 67 000 frames per second using a Phantom v12.0 digital camera running Phantom 692 software. Ignition time and temperature were then determined by mapping against the Callendar-Van Dusen temperature extrapolation from the temporal resistance of the Pt wire. T-Jump ignition experiments were performed in a pure $O_2$ environment at pressures ranging from 20.3 kPa to 1.89 MPa and under vacuum (∼0.13 mPa).

### D. *Ex situ* and *in situ* high heating rate TEM

High heating rate studies in a TEM were conducted with Protochips Aduro heating chips with a Protochips TEM holder in a JEM 2100 field emission gun (FEG) TEM/scanning transmission electron microscope (STEM), equipped with Oxford energy dispersive spectrometry (EDS) and Gatan Tridiem electron energy loss (EELS) systems, with an accelerating voltage of 200 kV. Ta nanopowders were deposited onto an Aduro chip and heated in air, whereas the Ta based

nanothermites were heated under vacuum within the TEM. All samples were heated at $10^5$ K/s and held for a period between 1 and 100 ms.

### E. Combustion cell characterization

Ta/CuO nanothermite was evaluated using a previously described combustion cell.[23] 25 mg of sample was placed in the ∼13 $cm^3$ cell and ignited by a resistively heated nichrome wire. An oscilloscope was used to record simultaneous pressurization and optical emission from a pressure transducer and a photomultiplier tube, respectively.

## III. RESULTS AND DISCUSSION

### A. Oxidation of nTa by gas phase oxygen

#### 1. TGA/DSC oxidation analysis

The oxidation of nTa was first studied using standard slow heating rate TGA/DSC under an $O_2$ flow (Fig. 1).

In the case of nTa, oxidation is a 1 step process beginning at ∼300 °C and ending at ∼500 °C. The exotherm occurring slightly above 600 °C possibly corresponds to the crystallization of $Ta_2O_5$ as the mass stays constant during this event. Complete oxidation of nTa would result in a final weight percent of ∼115%, indicating the nTa contains ∼70% unoxidized Ta before heating, as shown in Fig. 1(a). The onset temperature for oxidation is much lower for nTa (∼300 °C) than for nAl (∼600 °C), but the initial exotherm corresponding to oxidation occurs much more rapidly in the nAl case. This can be attributed to the outward diffusion of Al from the core when near the melting point of Al (660 °C). Trunov *et al.* have described the oxidation of nAl at slow heating rates as being a 4-step process with the predominant mass increases occurring in steps 3 and 4 corresponding to the growth of $\gamma$ and $\alpha$ phase $Al_2O_3$, respectively.[7] nTa does not appear to follow this multi-step oxidation mechanism as there is only a single stage of mass gain during the course of heating.

In the TGA/DSC analysis of nTa oxidation, both the fuel and metal oxide product are immobile in the temperature range of the experiment. Al begins to rapidly oxidize near the Al melting point (660 °C) due to the increased diffusion rates of liquid Al allowing for enhanced outward diffusion of Al through the nascent oxide shell. With Ta and $Ta_2O_5$ being immobile during the course of heating, oxidation must occur strictly by diffusion of $O_2$ through the oxide shell at slow heating rates. However, nTa undergoes a rapid self-sustaining oxidation when heated quickly which is not well captured using slow heating rate analytics such as TGA/DSC.

#### 2. T-Jump ignition in oxygen

The ignition behavior of pure nTa at various pressures of $O_2$ was analyzed using the T-jump heating technique coupled with high speed videography. The measured ignition temperatures as a function of $O_2$ pressure are shown in Fig. 2.

The measured ignition temperatures are much lower than those of nAl at the same pressures using an identical technique.[12] With Ta having such a high melting temperature, the
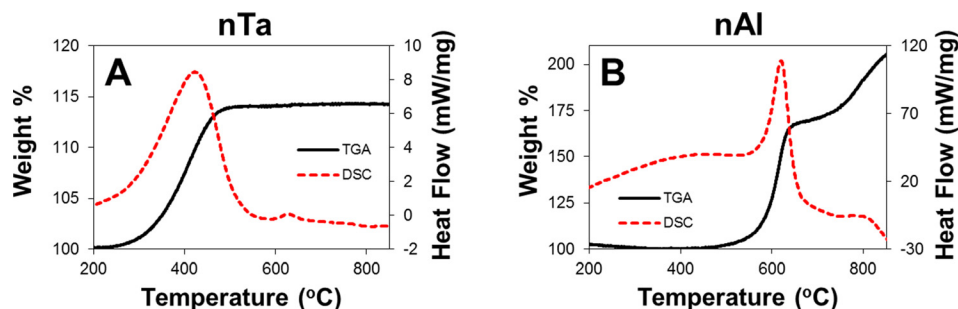
FIG. 1. TGA/DSC of nTa (a) and nAl (b) under 100 ml/min of $O_2$ at a heating rate of 20 °C/min.

reaction must be heavily dependent on the diffusion of oxygen through the oxide shell to the Ta core. The nascent $Ta_2O_5$ shell on nTa has a melting point of 1872 °C, which is more than 1000 °C higher than the measured ignition temperatures. This suggests that something must happen to this shell to allow for enhanced diffusion rates of gaseous oxygen and the ignition event, leading to self-sustained oxidation of the Ta core. As stated above, Kim and Stebbins have shown that amorphous $Ta_2O_5$ films will crystallize above 500 °C;[17] thus, it is reasonable to conjecture that the exothermic crystallization of $Ta_2O_5$ allows for enhanced diffusion of oxygen to Ta across the $Ta_2O_5$ boundary. This can be thought of as being similar to the hot spot ignition theory for CHNO energetics where localized points can begin to react exothermically, leading to a self-propagating reaction of the bulk material.[24] Potentially, only one point may rapidly crystallize, exposing the Ta core aiding in the rapid oxidation of Ta. The heat generated during the rapid oxidation will contribute to the further crystallization, and at a potential a temperature spike to enable melting of $Ta_2O_5$, exposing more of the Ta core. This theory was further explored using high heating rate TEM.

### 3. High heating rate TEM of nTa

In order to probe the oxidation mechanism of nTa, the growth of the $Ta_2O_5$ oxide shell was investigated by depositing nTa onto Protochips Aduro heating chips. First, the chip was inserted into the Protochips TEM holder, multiple particles were imaged, and positions were recorded. In order to oxidize nTa, the holder was removed from the TEM and rapidly heated in air to 500 °C at a heating rate of $10^5$ K/s and held at this temperature for 10 ms. This process was repeated 4 times with re-insertion of the holder into the TEM to image

the particles after each stage of heating. During the last heating run, the chip was held at 500 °C for 100 ms. The results in Fig. 3 show oxide shell thickness growth for 7 different locations on a single Ta aggregate. It is apparent that there is a difference in the growth rate depending on the location on the aggregate.

No crystallization of $Ta_2O_5$ is observed after any of the consecutive heating ramps, which agrees with the results seen in the TGA/DSC experiment above. In the TGA/DSC, the $Ta_2O_5$ crystallization exotherm occurs above 600 °C.

Slow heating rate studies on the oxidation of bulk tantalum in air indicate that oxidation follows a linear rate law in the 500 °C–800 °C temperature range.[25] The experimental results for the average oxide shell growth over time in Fig. 3 appear to follow a linear-parabolic trend similar to the Deal-Grove (D-G) model for the oxidation of silicon.[26] The Deal-Grove model originally developed for oxidation of silicon shows growth following a linear growth rate at short timescales (thin oxide layer) and a parabolic growth rate for long oxidation times (thick oxide layer). This implies that oxidation is kinetically limited in the initial stages, but once the shell reaches a certain thickness, oxidation is diffusion limited as shown below
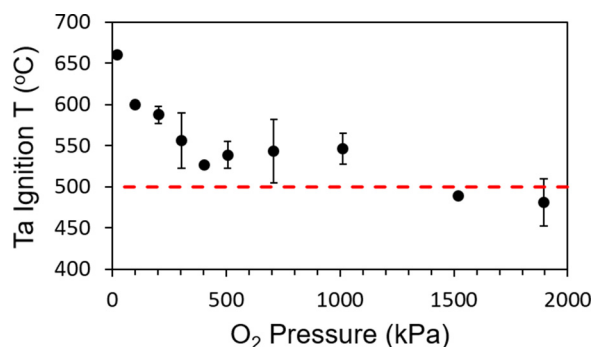




FIG. 2. Ignition temperature of nTa measured using the T-Jump ignition technique at varying $O_2$ pressures. The dashed line represents the crystallization temperature of $Ta_2O_5$ thin films.
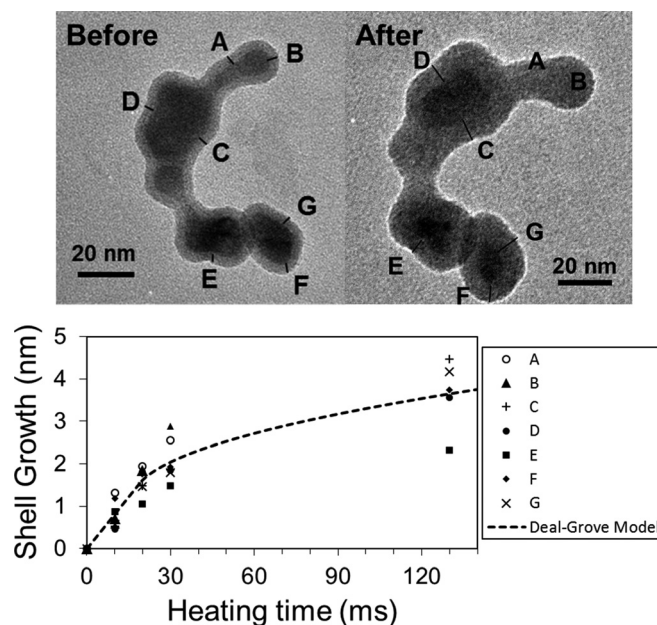
FIG. 3. TEM image of the Ta aggregate with labeled locations where the oxide shell was measured before and after heating and the corresponding heating time vs. oxide shell growth for each location along with a linear-parabolic fit of average shell growth following the Deal-Grove model.

$$\text{Linear Region}: Z = kC_s\tilde{v}t, \tag{1}$$

$$\text{Parabolic Region}: Z^2 = 2DC_s\tilde{v}t, \tag{2}$$

where $Z$ is the oxide shell thickness, $C_s$ is the molar concentration of oxygen at the surface of the material, $\tilde{v}$ is the molar volume of the formed metal oxide, $t$ is the time, and $k$ and $D$ represent the rate constant in the linear region and diffusion coefficient of $O_2$ in the formed metal oxide, respectively. Since both Si and Ta are immobile during the temperature range of oxidation and presuming no other factors come into play, D-G should be applicable to the Ta system. For the rapid heating of nTa in air to $500\,^\circ$C shown in Fig. 3, the linear to parabolic transition occurs after $\sim$1.62 nm of shell growth (20 ms of total heating). The rate constant for the linear region, $k$, is determined to be 160.4 nm/ms. A diffusion coefficient, $D$, of $52\,\text{nm}^2$/ms ($5.2 \times 10^{-14}\,\text{m}^2$/s) was extrapolated from the parabolic portion of the plot.

A previous study on the diffusion of oxygen in amorphous $Ta_2O_5$ thin films (100 nm thickness) reported a diffusion coefficient of $2.5 \times 10^{-19}\,\text{m}^2$/s at $\sim$525 $^\circ$C.[27] Our extrapolated value for oxygen diffusion through the oxide shell of nTa is more than 5 orders of magnitude larger. This is most likely due to the previous study being done on compact $Ta_2O_5$ films, while our oxygen diffusion coefficient was determined during oxidation of nTa and therefore more accurately represents oxygen diffusion during combustion.

Drastic surface changes of the oxide shell are clearly seen in Fig. 4, when Ta nanoparticles are heated in air to $850\,^\circ$C and held at temperature for 1 ms. A temperature of $850\,^\circ$C was chosen as the final temperature to ensure that all analyzed particles were sufficiently heated above $500\,^\circ$C with only 1 ms of hold time, as a result of heat losses from the chip when heated in air. During oxidation, the particle's outer diameter increased from 32.83 to 38.16 nm, while the Ta core shrank by nearly 4 nm. This particle diameter growth is due to the density of $Ta_2O_5$ being approximately half that of the Ta metal core (8.2 g/cm$^3$ vs. 16.7 g/cm$^3$, respectively). After rapid heating to $850\,^\circ$C, the oxide shell grew $\sim$4.6 nm over 1 ms. After 130 ms of total heating to $500\,^\circ$C, the average shell growth was only $\sim$3.7 nm.

A crack observed in the post-heating TEM image in Fig. 4(d) is further evidence that changes in the oxide shell may be enhancing oxidation rates. The rapid crystallization and the stress on the particle may cause the observed cracking of the shell, which can enhance oxygen diffusion into the core. Elemental compositions from EDS point scans in Fig. 4 show that no oxygen exists in the center of the particle (a) prior to heating in air. After heating, a significant increase in the percentage of oxygen is observed in both the edge (b) and center (c) of the particle. As oxidation occurs, it is possible that local temperatures may reach the melting point of $Ta_2O_5$, explaining the lack of multiple cracks in the shell in the post-heating TEM images. Localized melting of $Ta_2O_5$ would seal the crack, but as this newly formed amorphous oxide crystallizes, new cracks may form.

The above D-G model shows that oxidation is kinetically limited when the oxide shell is sufficiently thin. If we assume that cracking of the shell prevents the reaction from proceeding to the diffusion limited regime, we can calculate the effective activation energy for oxidation using the calculated rate constant for the linear region and the Arrhenius equation. The relative time required to heat the particles to $850\,^\circ$C at $10^5$ K/s with a 1 ms hold is significant in contrast to rapid heating to $500\,^\circ$C and holding for 10 ms. Theoretical shell growth, assuming a kinetically limited oxidation mechanism, during the course of the entire heating to the $850\,^\circ$C experiment is shown in Fig. S1 (supplementary material). Iterative calculations determined that $E_a$ required to match the experimentally measured shell growth of 4.6 nm is $\sim$65 kJ/mol (0.674 eV).

Selected area diffraction (SAD) patterns before and after rapid heating are shown in Fig. 5. Before heating, crystalline Ta from the core of the particle is observed, but no crystalline $Ta_2O_5$ is apparent. After heating, fringe lines corresponding to both crystalline Ta and crystalline $Ta_2O_5$ are visible. The clustered $Ta_2O_5$ fringe lines imply that the formed $Ta_2O_5$ has a preferred orientation with crystalline oxide growth occurring on specific planes.

High resolution TEM (HRTEM) images in Fig. 6(a) reveal little crystallization in the oxide shell after the series of heating ramps to $500\,^\circ$C (30 ms in total), but crystallization is clearly observed after being heated to $850\,^\circ$C for 1 ms in Fig. 6(b) (also confirmed by SAD in Fig. 5). These results show that rapid heating to $850\,^\circ$C results in a faster diffusion



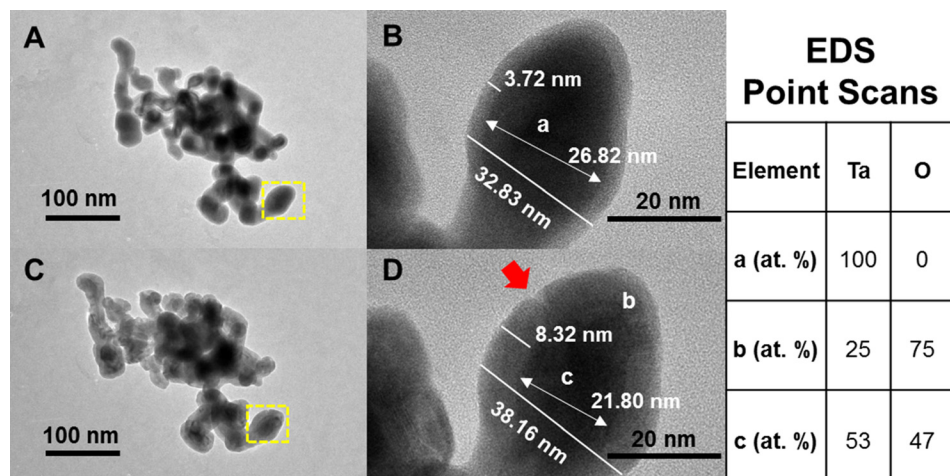| EDS Point Scans | | |
|---|---|---|
| Element | Ta | O |
| a (at. %) | 100 | 0 |
| b (at. %) | 25 | 75 |
| c (at. %) | 53 | 47 |

FIG. 4. TEM images before (a) and (b) and after (c) and (d) being heated in air to 850 $^\circ$C at $10^5$ K/s and held for 1 ms. EDS point scan atomic percentages of Ta and O at locations are labeled in (a) and (b). The arrow in (d) points to a crack in the oxide shell due to rapid crystallization.
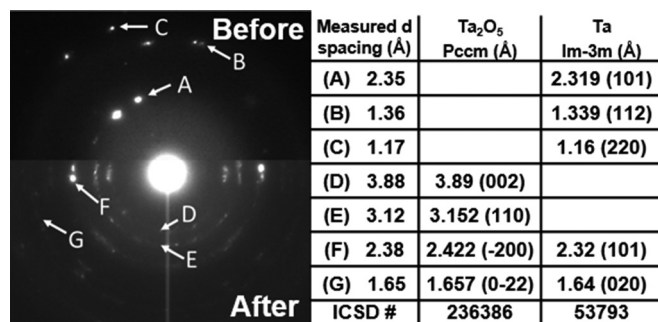
FIG. 5. SAD patterns of the particle shown in Fig. 4 before and after heating in air to 850 °C at $10^5$ K/s and held for 1 ms.

based oxidation mechanism that may be attributed to cracks forming in the oxide shell.

## B. Ta based nanothermites

### 1. T-Jump analysis of Ta based nanothermites

Various nTa based nanothermites were investigated using the same T-jump ignition technique as above. The ignition temperatures were measured in a vacuum environment ($\sim 10^{-6}$ torr) to eliminate the impact of ambient gas phase oxygen on ignition. The oxygen release temperature of the pure metal oxides was plotted vs. ignition temperature of nTa and nAl based thermites as shown in Fig. 7.

Ignition temperatures for the Ta based nanothermites appear to be independent of oxidizer type. In some cases, the ignition temperatures vary greatly from the corresponding Al based nanothermites, with the greatest disparity being between the $Fe_2O_3$ nanothermites. Post-combustion products from the T-Jump ignition in air of Ta/CuO nanothermite were imaged (Fig. S2 in the supplementary material) using a previously published method, and results are discussed in the supplementary material.[28] One important result not shown in Fig. 7 is that the Ta/$WO_3$ nanothermite did not ignite under these heating conditions ($\sim 24$ °C to $\sim 1200$ °C in 3 ms), but Al/$WO_3$ nanothermite has been previously shown to ignite at 757 °C in an identical setup.[10]

Table I shows the theoretical enthalpy of reaction per mole of metal fuel and adiabatic flame temperature for each nanothermite in Fig. 7. The theoretical adiabatic flame temperatures were calculated using the Cheetah 6.0 equilibrium code at a constant pressure.

The adiabatic flame temperatures are lower for all Ta based nanothermites, with the exception of the CuO containing
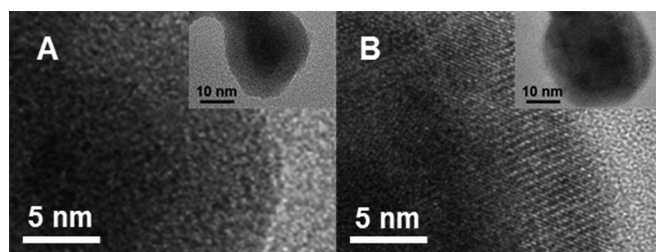


FIG. 6. HRTEM images of Ta nanoparticles after being heated in air to 500 °C multiple times (30 ms in total) (a) and to 850 °C for one time only (b), both at a heating rate of $10^5$ K/s.
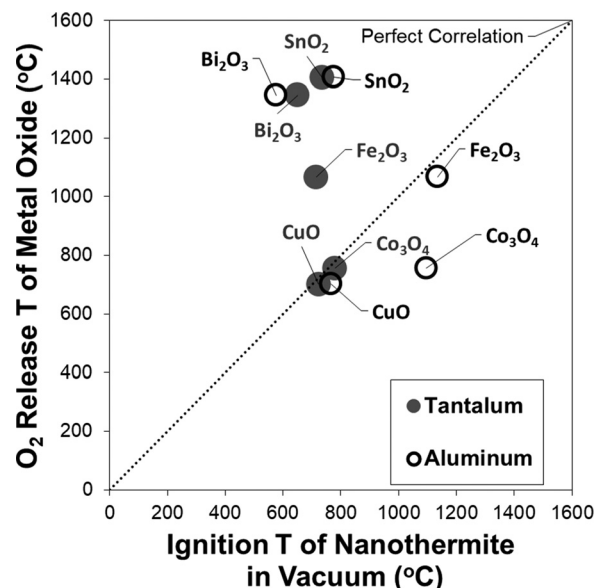


FIG. 7. Oxygen release temperature of pure metal oxide vs. ignition temperature of nTa and nAl based nanothermites.

nanothermite where the temperatures are approximately equivalent. There does not appear to be a trend between the enthalpy of reaction, $\Delta H_{rxn}$, and the ignition temperatures measured in Fig. 7. The Ta/$Fe_2O_3$ system has a lower $\Delta H_{rxn}$ than Al/$Fe_2O_3$ yet ignites at a lower temperature.

One possible explanation for the discrepancies in ignition temperatures of Ta and Al based nanothermites is that alloying reactions unique to the Ta system may decrease the onset temperature of reaction. A phase diagram for $Ta_2O_5$ and $Fe_2O_3$ generated using density functional theory (DFT) calculations shows that the $TaFeO_4$ alloy can be formed with an enthalpy of formation of $-2.5$ kJ/mol.[29–31] No stable alloy exists for the $Al_2O_3$/$Fe_2O_3$ system. Unfortunately, this pattern does not hold true for the $Co_3O_4$ containing thermites, which also show a large ignition temperature difference. Neither system forms a stable alloy with $Co_3O_4$; therefore, it is more likely that something unique to nTa and independent of the metal oxide is the cause for the trend in Fig. 7. As stated above, the Ta/$WO_3$ nanothermite did not ignite under these conditions, contradictory to previous studies on sol-gel derived Ta/$WO_3$ thermites that ignited between 465 and 670 °C.[18] This could be due to differences in the microstructure of the composite, heating environment, and heating rate. In addition, the sol-gel samples were pre-heated to 300–400 °C before ignition tests, and they also employed amorphous $WO_3$ where we used crystalline $WO_3$.

For each of the Ta based nanothermites, ignition occurs at or below the oxygen release temperature for the corresponding metal oxide. We propose that the metal oxide must wet the surface of the nTa for ignition to occur due to Ta being an immobile fuel under these conditions. Each of the Ta based nanothermites in Fig. 7 ignites fairly close to 700 °C, whereas the Al based nanothermites have a much wider range of ignition temperatures. The TGA/DSC results in Fig. 1(a) show an exotherm resulting from the crystallization of $Ta_2O_5$ with an onset temperature of 600 °C and peak temperature of 630 °C at low heating rates. The analysis of

TABLE I. Theoretical enthalpy of reaction per mole of metal fuel and adiabatic flame temperature calculated using the Cheetah 6.0 equilibrium code at constant pressure for each nanothermite.

|  | Ta | | Al | |
|---|---|---|---|---|
|  | $\Delta H_{rxn}$ (KJ/mol Ta) | Adiabatic flame temperature (K) | $\Delta H_{rxn}$ (KJ/mol Al) | Adiabatic flame temperature (K) |
| Cuo | −633 | 2842 | −604 | 2845 |
| $Fe_2O_3$ | −335 | 1963 | −425 | 3132 |
| $Co_3O_4$ | −455 | 2462 | −497 | 3169 |
| $SnO_2$ | −301 | 3290 | −405 | 3697 |
| $Bi_2O_3$ | −548 | 2283 | −553 | 3191 |
| $WO_3$[a] | −321 | … | −417 | … |

[a]$WO_3$ not in cheetah 6.0 database.

the crystallization of amorphous $Ta_2O_5$ thin films by Kim and Stebbins showed that crystallization rates rapidly increased at higher temperatures.[17] We propose that at high heating rates, the crystallization of the amorphous shell releases enough energy in a short amount of time at the nTa/metal oxide interface to initiate reaction between the fuel and the oxidizer. In the case of Al based thermite reactions, Al goes through an endothermic phase change (melting) near the crystallization temperature of its oxide shell. With $Al_2O_3$ making up only 19 wt. % of nAl, the net process in this temperature regime would be endothermic as energy released from crystallization would go into the melting of Al. For the Ta case, the metal core does not go through any phase changes near the crystallization temperature of the oxide shell; therefore, the energy released from crystallization will locally heat the particle. Similar conclusions on crystallization induced ignition were drawn by Cervantes *et al.* for the sol-gel derived Ta/$WO_3$ thermite system where they saw decreased ignition temperatures when amorphous $WO_3$ was employed.[20] These types of surface interactions were further probed using high-high heating rate TEM for Ta/$Fe_2O_3$ and Ta/CuO nanothermites below (Fig. 8).

### 2. High heating rate TEM of Ta based nanothermites

The Ta/$Fe_2O_3$ nanothermite system showed the largest disparity between nAl and nTa based systems, warranting a closer look at the reaction mechanism. Ta/$Fe_2O_3$ nanothermite was heated in the TEM at $10^5$ K/s to 1200 °C and held for 1 ms. Sullivan *et al.* preformed a similar study using the same *in-situ* high heating rate TEM technique with an Al
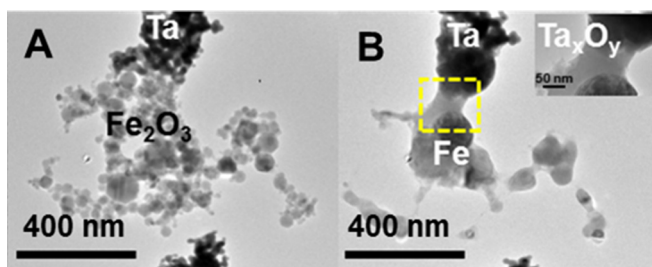


FIG. 8. TEM images of Ta/$Fe_2O_3$ nanothermite before (a) and after (b) being heated to 1200 °C at a heating rate of $10^5$ K/s and held for 1 ms and the HRTEM image of the interface after heating (inset).

based thermite system, and a reactive sintering reaction mechanism was supported.[8] Figures 8(a) and 8(b) show before and after heating TEM images where $Fe_2O_3$ appears to wet the surface of Ta to allow for oxygen to diffuse through the $Ta_2O_5$ shell to oxidize Ta. Unlike Al, Ta does not sinter at areas that are not in contact with $Fe_2O_3$ under these heating conditions as shown by the maintained nanostructure of parts of the Ta aggregate shown in Fig. 8(b), which again proves that wetting the Ta fuel surface by the oxidizer is crucial for its ignition. The added heat at the interface may be promoting the reactive sintering between nTa and $Fe_2O_3$.

Ta/CuO nanothermite was also rapidly heated in the TEM to 1200 °C at a heating rate of $10^5$ K/s and held for 10 ms. TEM images shown in Fig. S3 (supplementary material) show a similar "wetting" phenomenon as seen in the Ta/$Fe_2O_3$ system. EDS results show that that CuO is fully reduced to Cu and even at a location away from the interface, Ta is oxidized, showing the ability for oxygen to be transported throughout the Ta aggregate, even in a vacuum environment.

### 3. Modeling the burn time of Ta/CuO nanothermite

Using our experimentally determined activation energy for oxidation (65 kJ/mol) described above, a kinetically limited shrinking core model was employed to determine a theoretical burn time for a stoichiometric Ta/CuO nanothermite. We primarily chose a shrinking core based on our prior studies on size resolved measurements on the burn rate of nanoscale titanium and zirconium particles.[32] The model derivation is outlined in Ref. 33, and the final equation can be stated as

$$\rho_{Ta} \frac{dr_c}{dt} = -bkC_{O2}, \qquad (3)$$

where $\rho_{Ta}$ is the molar density of tantalum, $r_c$ is the radius of the unreacted core, $k$ is the reaction rate constant, $C_{O2}$ is the concentration of the gaseous oxidizer, and $b$ is the stoichiometric coefficient of Ta in the oxidation reaction normalized per mole of oxidizer ($0.8Ta + O_2 \rightarrow 0.4Ta_2O_5$). The oxygen concentration used in the model was determined from the full decomposition of the metal oxide (CuO in this case). The model assumes that oxidation of Ta is a kinetically limited process and the timescale of oxygen release from CuO is negligible. The experimental burn time was obtained from evaluating the burn time within a fixed volume combustion cell. The amount of CuO used defines the totally available oxygen initially.

For our calculations, we assumed a 33 nm nTa particle as depicted in Fig. 5. We also ignored heat losses from convection and radiation but limited the maximum achieved temperature to the adiabatic flame temperature for Ta/CuO (2842 K) as shown in Table I. The rate constant at each time step in the model was calculated using the Arrhenius equation below with the experimentally determined activation energy of 65 kJ/mol

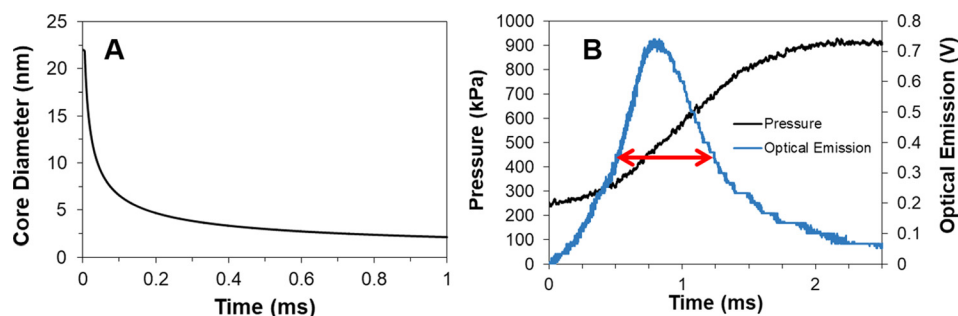$$k = k_o e^{-E_a/(k_B T)}, \qquad (4)$$

FIG. 9. Kinetically limited shrinking core model for reaction using the $E_a$ of 65 kJ/mol (a) and combustion cell experimental results (b) with the arrow labeling full width half maximum (FWHM) for the Ta/CuO nanothermite reaction.

where $k$ is the reaction rate coefficient at a given temperature, $E_a$ is the activation energy for oxidation, $k_B$ is the Boltzmann constant, and $T$ is the temperature. The maximal reaction rate coefficient, $k_o$, of $3.96 \times 10^6$ nm/ms was determined from the value extrapolated from successive heating to 500 °C and single heating ramp to 850 °C. The oxygen concentration used in the model was determined by using a stoichiometric amount of CuO in the combustion cell with a total nanothermite mass of 25 mg and a volume of 13 cm$^3$. The oxygen content in the model was finite; therefore, oxygen concentration decreased as it was consumed by nTa. The model results and combustion cell experimental results are shown in Fig. 9.

The kinetically limited shrinking core model shows that the core diameter has shrunk by ∼90% in 0.9 ms [Fig. 9(a)]. The FWHM of the optical emission from the combustion cell experiment, commonly used as the burn time, shows a duration of ∼0.8 ms [Fig. 9(b)], which suggests that a shrinking core model reasonably captures the reaction time for Ta high temperature oxidation based on parameters extracted at low temperature *Deal-Grove* oxidation.

### C. nTa oxidation mechanism summary

Two distinct nTa oxidation mechanisms are apparent for nTa reacting with gas phase oxygen: a slow heating rate, low temperature oxidation resulting in the formation of amorphous Ta$_2$O$_5$, and a rapid oxidation caused by the crystallization of amorphous Ta$_2$O$_5$ creating cracks in the shell.

The Ta nanothermite reaction mechanism is controlled by reactive sintering with metal oxide. The metal oxide must "wet" Ta because Ta is immobile in the temperature range of ignition. Rapid crystallization of the oxide shell leads to heat release at the interface promoting sintering with the metal oxide. nAl also undergoes crystallization of its oxide shell, but the net energy at the interface is endothermic due to the melting of the Al core, which makes up 81% of the mass of a nAl particle. The exothermic crystallization of the Ta$_2$O$_5$ shell (Fig. 1) may be attributing to the initiation of localized reactive sintering with Fe$_2$O$_3$. This could also explain the trend in ignition temperatures seen in Fig. 7 where the ignition temperature for nTa based thermites seems to be independent of the metal oxide employed.

## IV. CONCLUSION

This study probed the importance of oxide shell crystallization in the oxidation mechanism of Ta nanoparticles and nanothermites. High heating rate TEM analysis showed that oxide shell growth occurred slowly when heated in air below 500 °C and was amorphous. When heated in air to 850 °C, oxide shell growth happened rapidly and crystallization of the shell led to cracks that may attribute to the enhanced oxygen diffusion rates. When investigating the nTa oxidation mechanism with a condensed phase oxidizer, ignition temperatures were independent of the employed metal oxide, unlike corresponding Al nanothermites. We propose that the rapid oxide shell crystallization of nTa contributes enough energy to the shell/oxidizer interface that reactive sintering is induced and kinetically limited oxidation occurs. An activation energy for oxidation was experimentally determined to be 65 kJ/mol from the D-G model and was used to model the burn time of the Ta/CuO nanothermite system.

## SUPPLEMENTARY MATERIAL

See supplementary material for a figure (Fig. S1) showing the theoretical shell growth of nTa using the kinetically limited portion of the Deal-Grove model using an activation energy of 65 kJ/mol. There is also a discussion on T-Jump product collection and SEM images of Ta/CuO nanothermite combustion products (Fig. S2). Figure S3 shows TEM images before and after heating of Ta/CuO nanothermite in addition to EDS results.

[1] E. L. Dreizin, Prog. Energy Combust. Sci. **35**(2), 141–167 (2009).
[2] N. H. Yen and L. Y. Wang, Propellants, Explos., Pyrotech. **37**(2), 143–155 (2012).
[3] L. L. Wang, Z. A. Munir, and Y. M. Maximov, J. Mater. Sci. **28**(14), 3693–3708 (1993).
[4] M. R. Weismiller, J. Y. Malchi, J. G. Lee, R. A. Yetter, and T. J. Foley, Proc. Combust. Inst. **33**, 1989–1996 (2011).
[5] S. Chowdhury, K. Sullivan, N. Piekiel, L. Zhou, and M. R. Zachariah, J. Phys. Chem. C **114**(20), 9191–9195 (2010).
[6] V. I. Levitas, Combust. Flame **156**(2), 543–546 (2009).
[7] M. A. Trunov, M. Schoenitz, and E. L. Dreizin, Combust. Theory Modell. **10**(4), 603–623 (2006).
[8] K. T. Sullivan, N. W. Piekiel, C. Wu, S. Chowdhury, S. T. Kelly, T. C. Hufnagel, K. Fezzaa, and M. R. Zachariah, Combust. Flame **159**(1), 2–15 (2012).
[9] A. Rai, K. Park, L. Zhou, and M. R. Zachariah, Combust. Theory Modell. **10**(5), 843–859 (2006).
[10] G. Jian, S. Chowdhury, K. Sullivan, and M. R. Zachariah, Combust. Flame **160**(2), 432–437 (2013).

[11]V. I. Levitas, B. W. Asay, S. F. Son, and M. Pantoya, Appl. Phys. Lett. **89**(7), 071909 (2006).

[12]W. Zhou, J. B. DeLisio, X. Wang, G. C. Egan, and M. R. Zachariah, J. Appl. Phys. **118**(11), 114303 (2015).

[13]G. C. Egan, K. T. Sullivan, T. LaGrange, B. W. Reed, and M. R. Zachariah, J. Appl. Phys. **115**(8), 084903 (2014).

[14]G. C. Egan, T. LaGrange, and M. R. Zachariah, J. Phys. Chem. C **119**(35), 20401–20408 (2015).

[15]E. L. Dreizin, Prog. Energy Combust. Sci. **26**(1), 57–78 (2000).

[16]D. A. Firmansyah, T. Kim, S. Kim, K. Sullivan, M. R. Zachariah, and D. Lee, Langmuir **25**(12), 7063–7071 (2009).

[17]N. Kim and J. F. Stebbins, Chem. Mater. **23**(15), 3460–3465 (2011).

[18]J. D. Kuntz, O. G. Cervantes, A. E. Gash, and Z. A. Munir, Combust. Flame **157**(8), 1566–1571 (2010).

[19]O. G. Cervantes, J. D. Kuntz, A. E. Gash, and Z. A. Munir, Combust. Flame **157**(12), 2326–2332 (2010).

[20]O. G. Cervantes, J. D. Kuntz, A. E. Gash, and Z. A. Munir, Combust. Flame **158**(1), 117–122 (2011).

[21]L. Zhou, N. Piekiel, S. Chowdhury, and M. R. Zachariah, Rapid Commun. Mass Spectrom. **23**(1), 194–202 (2009).

[22]G. Jian, N. W. Piekiel, and M. R. Zachariah, J. Phys. Chem. C **116**(51), 26881–26887 (2012).

[23]K. Sullivan and M. R. Zachariah, J. Propul. Power **26**(3), 467–472 (2010).

[24]G. Levesque, P. Vitello, and W. M. Howard, J. Appl. Phys. **113**(23), 233513 (2013).

[25]V. B. Voitovich, V. A. Lavrenko, V. M. Adejev, and E. I. Golovko, Oxid. Met. **43**(5–6), 509–526 (1995).

[26]B. E. Deal and A. S. Grove, J. Appl. Phys. **36**(12), 3770 (1965).

[27]R. Nakamura, T. Toda, S. Tsukui, M. Tane, M. Ishimaru, T. Suzuki, and H. Nakajima, J. Appl. Phys. **116**(3), 033504 (2014).

[28]R. J. Jacob, G. Q. Jian, P. M. Guerieri, and M. R. Zachariah, Combust. Flame **162**(1), 258–264 (2015).

[29]A. Jain, O. Shyue Ping, G. Hautier, W. Chen, W. D. Richards, S. Dacek, S. Cholia, D. Gunter, D. Skinner, G. Ceder, and K. A. Persson, Appl. Mater. **1**(1), 011002 (2013).

[30]S. P. Ong, L. Wang, B. Kang, and G. Ceder, Chem. Mater. **20**(5), 1798–1807 (2008).

[31]A. Jain, G. Hautier, S. P. Ong, C. J. Moore, C. C. Fischer, K. A. Persson, and G. Ceder, Phys. Rev. B **84**(4), 045115 (2011).

[32]Y. C. Zong, R. J. Jacob, S. Q. Li, and M. R. Zachariah, J. Phys. Chem. A **119**(24), 6171–6178 (2015).

[33]F. Gao, P. Kar, K. Wang, and H. Liang, in *Proceedings of the STLE/ ASME International Joint Tribology Conference 2008* (2009), pp. 727–729.